A Hypersonic Plasma Power Generator

K. J. TOURYAN*
Sandia Laboratory, Albuquerque, N. Mex.

Theoretical and experimental analyses are presented which describe the operation and characteristics of a hypersonic plasma generator. The nose cone of a re-entry vehicle serves as a thermionic emitter of electrons (a cathode). These electrons are then conducted through the shock ionized air stream, increased in kinetic energy by collisions, and collected over the relatively cool vehicle afterbody, which is electrically insulated from the nose cone and which serves as an anode, or collector. A load connected between the cathode and anode within the vehicle completes the circuit. The generator operates basically as a plasma thermocouple and, for its power output, depends primarily on the large temperature and area differences between emitter and collector, with the kinetic energy of the plasma electrons as its energy source. Experiments in a plasma tunnel facility have yielded currents up to 30 amp/in.^{2} of emitter area (pyrographite or graphite surfaces) under short-circuit and fully charge-neutralized conditions and 4.0 v open-circuit voltage and 1-ev plasma electron temperatures (16 w/in.^{2} power output). Conditions for optimum output are discussed and estimates made for full-size re-entry vehicles on the basis of detailed re-entry trajectory calculations.

Nomenclature

A	=	const, $4\pi m_e k^2/h^3$
A_e (or A_{em}), A_c	=	emitter and collector areas, respectively, in.^{2}
C	=	$\alpha R I_{th}/\sigma V_T$
$\bar{c}_i$	=	thermal velocity, fps
D	=	diffusion coefficient
E	=	emf or electric field, v
e	=	electronic charge, 1.60207×10^{-19} coul
h	=	Planck's constant
I	=	current, amps
i	=	I/I_{th}
i_m	=	maximum value of i
j or J	=	current density, amps/unit area
k	=	Boltzmann constant, 1.3709×10^{-16} erg/deg
l	=	length
m_e, m_i	=	electronic and ionic mass, respectively
n_e, n_i	=	electron and ion number densities, respectively
R_l	=	load resistance
r	=	resistivity
T	=	temperature
T_e, T_{em}, T_c	=	electron, emitter, and collector temperatures, respectively
v	=	velocity
V	=	potential, v
V_T	=	plasma temperature equivalent potential
α	=	a number less than one, Eq. (31)
β	=	a ratio, $I_{eem}/I_{ec} \sim A_e/A_c$
γ	=	a ratio $I_{ic}/I_{ec} \sim 1/155$ for air
δ	=	a ratio I_{th}/I_{eem}
η	=	efficiency
E	=	thermocouple emf
λ	=	mean free path
θ	=	spherical coordinate or angle from horizontal
Θ	=	thermoelectric power
ρ	=	reflection coefficient
μ	=	mobility
σ	=	electrical conductivity
ϕ	=	work function

Subscripts

e, i, p	=	plasma electron, plasma ions, and general plasma conditions
em	=	emitter conditions
c	=	collector conditions
oc	=	open-circuit
sc	=	short-circuit
m	=	maximum

Presented as Preprint 64-449 at the 1st AIAA Annual Meeting, Washington, D. C., June 29–July 2, 1964; revision received January 11, 1965. This work was supported by the U. S. Atomic Energy Commission. Reproduction in whole or in part is permitted for any purpose of the U. S. Government.

* Staff Member, Aerophysics Section. Member AIAA.

Introduction

DIRECT conversion of thermal energy to electrical energy without need of intermediate mechanical conversion has a unique adaptability to space flight conditions and promises to be an attractive means of power generation. Much research has been done to develop such devices, among which are the thermionic converters (vacuum diodes, plasma diodes) and the thermoelectric systems (thermocouple, plasma generator). Thermionic converters have been discussed extensively in the literature.[1–4] The principle involved here is that heat applied to an emitter, or cathode, enables electrons to overcome the emitter work functions ϕ_{em} or the energy required to bring a conduction (Fermi level) electron to rest outside the emitter. The electron then travels through vacuum or a cesium plasma, depending on whether it is a vacuum diode or a plasma diode, to a collector, or anode, which has a lower work function ϕ_c. Because of this lower work function, electrons entering the collector can flow through a retarding potential $V = \phi_{em} - \phi_c$ in a load circuit before returning to the emitter. The emitter is usually a metallic surface of low work function, which emits electrons according to the Richardson-Dushman equation

$$J = AT_{em}^2 \exp(-e\phi_{em}/kT_{em})$$

The interelectrode plasma usually consists of an easily ionizable gas, such as cesium, serving the dual purpose of neutralizing the space-charge when the electron emission exceeds saturation quantities (see Fig. 1), lowering the emitter surface work function by forming a monolayer on the surface. To minimize losses from collisions between emitted electrons and the plasma, the plasma is kept at a density low enough to insure mean free paths larger than the interelectrode spacing.

The plasma generator[5] depends for its power output primarily on the large temperature and area differences between emitter and collector, and, unlike the thermionic converter, whose source of energy is the kinetic energy of electrons ($=2kT_e$) escaping from the hot emitter, the plasma converter depends on the kinetic energy of the plasma electrons for its source of energy. Since plasma electron temperatures can be

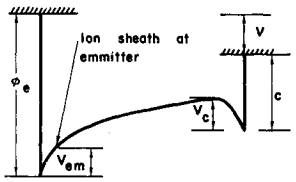

Fig. 1 Potential diagram of plasma generator, space-charge neutralized.

many times higher than the hottest practicable emitters, the latter is, compared to the thermionic converter, a high-voltage device. Physically then, the plasma converter operates as a thermocouple with the plasma operating as one branch and the emitter collector as the other.

This phenomenon has been used in a recent investigation by LeBlanc[6] to describe a power generation technique in which hot plasma is obtained behind the ionizing bow shock of a hypersonic vehicle in a re-entry trajectory. Figure 2 indicates such a vehicle with the nose cone serving as a hot emitter and the afterbody as a relatively cool collector separated by a thin electrical insulator. The emitted electrons are conducted through the shock ionized air stream, increased in kinetic energy by collisions, and collected over the collector. A load connected between the cathode and the anode within the vehicle completes the circuit. Of course, such a thermocouple or plasma generator is not a direct converter of heat energy to electrical energy, but it operates as a heat engine with heat rejection from the collector (see details in Sec. IC).

First initiated at Los Alamos Scientific Laboratory (LASL) by T. Cotter, work on such a generator has since been carried out by the Aerophysics Section, with the cooperation of the Electrical Engineering Department of the University of New Mexico under two contracts with the Sandia Corporation. The work done on the generator, so far, is contained in Refs. 6–9.

I. Theory

A. Current-Voltage Characteristics

To understand the operation of a plasma generator, the reader is referred to the potential diagram in Fig. 1. It is seen from Fig. 1 that the output voltage will be given by

$$V = \phi_{em} - \phi_c - V_{em} + V_c - Ir \qquad (1)$$

where V_{em} and V_c are the sheath potentials at the emitter and the collector, respectively, and Ir is the circuit impedance (both internal and external).

The net current flowing through the device can be expressed at the emitter side in terms of the emission current I_{th}, random electron current I_{eem} and ion current, I_{iem}. Using the notation of Ref. 5, at the emitter,

$$\left.\begin{aligned} I &= I_{th} + I_{iem} - I_{eem}\exp(eV_{em}/kT_{e1}) \quad V_{em} < 0 \\ I &= I_{th}\exp(-eV_{em}/kT_{em}) - I_{eem} \quad V_{em} > 0 \end{aligned}\right\} \qquad (2)$$

Similarly, at the collector,

$$\left.\begin{aligned} I &= I_{ec}\exp(eV_{ec}/kT_{e2}) - I_{ic} \quad V_c < 0 \\ I &= I_{ec} \quad V_c > 0 \end{aligned}\right\} \qquad (3)$$

In the preceding, T_{e1} and T_{e2} are the plasma electron temperatures in the vicinity of the emitter and collector, respectively.

Around a re-entry vehicle, $T_{e1} > T_{e2}$. Combining Eqs. (1–3) for the space-charge neutralized case, the generator voltage can be expressed by

$$V = V_{T_{e1}}\ln\frac{\{[n_{e2}eA_c/(I+I_{ic})](kT_{e2}/2\pi m_e)^{1/2}\}^{1/T_r}}{\{[n_{e1}eA_{em}/(I_{th}+I_{iem}-I)](kT_{e1}/2\pi m_e)^{1/2}\}} + \phi_{em} + \phi_c - Ir \qquad (4)$$

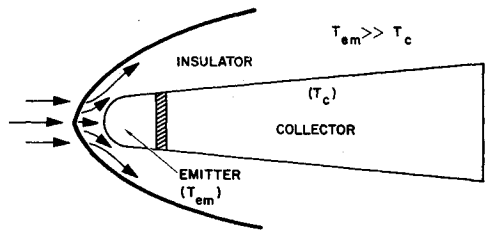

Fig. 2 Schematic of plasma generator.

where $T_r = T_{e1}/T_{e2}$. To simplify Eq. (4), we assume $T_{e1} \cong T_{e2}$ and obtain

$$V = V_{T_{e1}}\ln\left[\frac{I_{ec}}{I_{eem}}\left(\frac{I_{th}+I_{iem}-I}{I_{ic}+I}\right)\right] + \phi_{em} - \phi_c - Ir \qquad (5)$$

Equation (5) is represented graphically in Fig. 3 with some experimental results. In a plasma generator, the first term on the right becomes the dominant term for $T_e \geq 1$ ev (11,600°K) and $I_{ec}/I_{eem} \gg 1$. For low temperature plasmas, such as in the cesium diode, the second term ($\phi_{em} - \phi_c > 0$) becomes the main source of voltage output. The respective random electron currents at the emitter and collector can be given by

$$I_{eem} = A_{em}n_{e1}e\left(\frac{kT_{e1}}{2\pi m_e}\right)^{1/2}\exp\left(\frac{-eV_{em}}{kT_{e1}}\right) \qquad (6)$$

$$I_{ec} = A_c n_{e2}e\left(\frac{kT_{e2}}{2\pi m_e}\right)^{1/2}\exp\left(\frac{-eV_c}{kT_{e2}}\right) \qquad (7)$$

Taking the ratios of (6) and (7), one has

$$\frac{I_{ec}}{I_{eem}} = \left(\frac{A_c}{A_{em}}\right)\left(\frac{n_{e2}}{n_{e1}}\right)\left(\frac{T_{e2}}{T_{e1}}\right)^{1/2}\exp\left[\frac{e}{k}\left(\frac{V_c}{T_{e2}} - \frac{V_{em}}{T_{e1}}\right)\right] \qquad (8)$$

In Eq. (8), one can approximately represent the random electron current ratios as a function of the collector-to-emitter area ratio:

$$I_{ec}/I_{eem} \cong A_c/A_{em} = 1/\beta$$

This really will be valid for $V_c/T_{e2} > V_{em}/T_{e1}$, which will render the exponential term greater than one and thus offset the product of the electron density ratio and temperature ratio, which is always less than one. Thus, a large collector-to-emitter area ratio will also add to the power output. The Ir term is the internal impedance of the generator and is composed of the plasma resistance and the internal "contact" resistances.

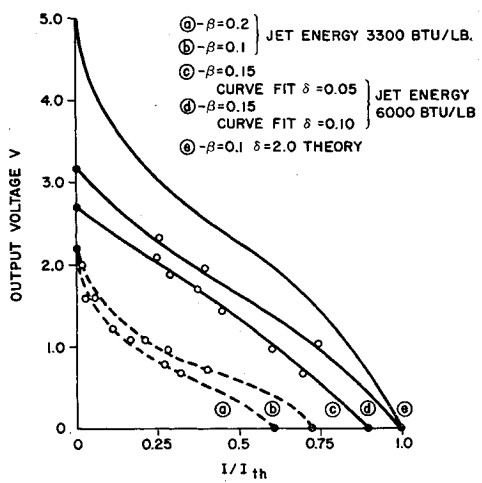

Fig. 3 Voltage-current characteristics for V_T = 1.0, and for various β and δ values in argon gas.

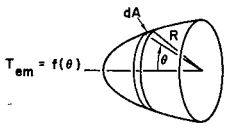

Fig. 4 Emitter geometry and coordinate system.

From Eq. (5), the open-circuit voltage will yield

$$V_{0c} = \frac{kT_e}{e} \ln\left[\frac{J_{ec}}{J_{eem}}\left(\frac{J_{th} + J_{iem}}{J_{ic}}\right)\right] + \phi_{em} - \phi_c \qquad (9)$$

where the J's are current densities per unit area, indicating that V_{0c} is independent of generator size. In nondimensional form, Eq. (6) becomes

$$V_{0c} = V_T \ln[(1 + \gamma/\delta)/\gamma/\delta] + \phi_{em} - \phi_c \qquad (10)$$

where

$$\delta = J_{th}/J_{eem} \qquad \gamma = J_{ic}/J_{ec}$$

V_T = voltage equivalent of plasma temperature

For $V_{em} > 0$, the equivalent expression for the open-circuit voltage becomes

$$V_{0c} = V_{Tem} \ln\delta/\gamma + V_T \ln 1/\gamma + \phi_{em} - \phi_c \qquad (11)$$

where V_{Tem} is equal to the voltage equivalent of emitter temperature.

One can see from Eq. (11) that the output voltage, among other things, depends strongly on the plasma temperature and ionization level. The various terms in this equation are discussed more fully in Sec. II of this paper.

For $\phi_{em} - \phi_c \sim 0$ and $r = 0$, the short-circuit current is given by

$$I_{sc} = \frac{I_{th} + I_{iem} - (I_{ic} + I_{th}')\beta}{1 + \beta} = \frac{I_{th} - I_{th}'\beta}{1 + \beta} \qquad (12)$$

where $\beta = I_{eem}/I_{ec}$ and the back emission term I_{th}' also has been included. Neglecting back emission, one can see that the larger the emission current and the smaller β is, the higher the short-circuit current will be. Thus, both emitter area and emitter-to-collector area ratio enter as independent parameters governing the generator output.

B. Emitter and Collector Currents

A review of the various current terms used previously might shed some further insight into the operating principles of the hypersonic generator.

1. *Thermionic emission current* I_{th}

As given in the Introduction, I_{th} is the Richardson-Dushman current expressed in its simplest form as

$$I_{th} = AT_{em}^2 \exp\left(-\frac{e\phi_{em}}{kT_{em}}\right) \times \text{area} \qquad (13)$$

To apply this expression to actual emitters, one should take into consideration two major effects not shown in Eq. (13). The first is the temperature dependence of the work function $\phi_{em} = \phi_{em}(T = T_{ref}) + \alpha T$, where α is the temperature coefficient determined empirically, and the nonuniform temperature distribution over the emitter area, and the second is the nonexistence of so-called clean surfaces (no adsorption, completely uniform, single crystal orientation) for which the derivation of Eq. (13) is valid. The biggest indeterminate factor resulting from this nonuniformity is in the value of $A = 4\pi m_e k^2/h^3$, which gives 120 amp/cm^2-deg^2 as a theoretical value. These and other factors are discussed extensively in the literature,[1] and are summarized as follows: a) work function dependent on temperature; b) an effective A determined experimentally and possibly expressed as $A = A^*(1 - \rho)$, A^* being the theoretical value and ρ a reflection coefficient; c) nonuniform surface giving rise to "patch effects" with widely varying values of work functions; d) large variations in crystal orientations which in turn would cause very large emission current variations; e) adsorbed gases changing the effective surface work function by as much as 400%. A more sophisticated expression for Eq. (13) may be given by (see Fig. 4)

$$I_{th} = 240\pi R^2 \int_\theta (1 - \rho) T_{em}^2(\theta) \exp\left[-\frac{e\phi_{em}(T)}{kT_{em}}\right] \sin\theta \, d\theta \qquad (14)$$

where $T(\theta)$ is obtained from the aerodynamic heating calculations for a given re-entry condition and emitter geometry, and ρ is determined empirically.

2. *Emitter and collector ion currents*

The simplest expression for the ion current is given on the basis of random ion velocities

$$I_i = 1/4 n_i \bar{c}_i \times \text{area} \qquad (15)$$

I_i, or the ion arrival rate, governs the space charge formation at the anode or the cathode. To neutralize the excess negative charge from the emitted electron cloud, a certain number of ions will be necessary with their flow rate governed by their mobility relative to that of the electrons. Because the former is much heavier than the latter, fewer ions will be necessary to neutralize a given electron cloud. Mathematically, this may be expressed as

$$I_{ion}/I_{electron} = (m_e/m_i)^{1/2} \qquad (16)$$

Several assumptions have been made in the derivation of Eqs. (15) and (16), which need a critical evaluation to make them directly applicable to the hypersonic generator phenomenon. First, the directed velocity $\bar{v}_i$ of the ions should be taken in consideration

$$I_i = en_i[(2e/m_i)(E_p + E)]^{1/2} \times \text{area} \qquad (17)$$

where

$E_p = (1/e)(1/2m_i\bar{v}_i^2)$
E = potential at any point in the sheath

It can be shown[10] that this assumption leads to a modified form of Eq. (16)

$$I_i/I_e = (m_e/m_i)^{1/2} \times F(E_p) \qquad (18)$$

where $F(E_p)$ is a function of directed ion energies given by

$$F(E)_p = \frac{1 - (E_p/V_s)^{1/2}[1 + (kT_e/2E_p)] + (E_p/2V_s)}{1 - (\pi kT_{em}/4V_s)^{1/2} - [(kT_e - kT_{em})/2V_s]} \qquad (19)$$

where V_s is the potential at the sheath edge. For a given plasma temperature $F(E_p) < 1$ and, hence, there is a net reduction in the ion arrival rate. A second assumption involves the density of the gas surrounding the model. Both Eqs. (15) and (17) assume low-density, inertia controlled sheaths. For higher pressures, the ion flow is governed by diffusion and mobility, and thus

$$I_i = e[D_i \nabla n_i + \mu_i n_i E] \times \text{area} \qquad (20)$$

where μ_i is related to D_i by the Einstein relationship $D_i = \mu_i T_i$.

For a floating potential, one can show[11] from the ion and electron diffusion equation that $I_{ion} = \frac{1}{4} n\bar{c}_i[\frac{3}{4}(\lambda/R)]$, or that the ion current and consequently electron emission is reduced by a factor of the Knudsen number at the wall. Thus, at stagnation pressure where the mean free path is less than the Debye length, a drastic reduction in thermionic emission could occur, limiting the usefulness of the hypersonic generator to altitudes above 100,000 ft.

3. *Emitter and collector random electron currents*

Because of the much higher mobility of the electrons, a Maxwellian distribution will be a valid description. The random electron current is then given by

$$I_e = en_e\left(\frac{kT_e}{2\pi m_e}\right)^{1/2}\exp\left(-\frac{eV_{em}}{kT_e}\right)\times \text{area} \qquad (21)$$

for the space charge neutralized case, and by

$$I_e = en_e(kT_e/2\pi m_e)^{1/2}\times \text{area for } V_{em} > 0 \qquad (22)$$

where n_e is the plasma electron density for the space-charge controlled regime.

C. Thermodynamic Considerations

The plasma generator described previously has all of the essential elements of a thermocouple. The interface may be thought of as a junction between two conductors, the metal and an electron gas whose distribution is determined primarily by space charge. The addition of ions will reduce this charge to a minimum thickness and create a neutral plasma as discussed previously. Treating this as a thermocouple, it is then possible to analyze its behavior in terms of the thermoelectric power in its branches (Fig. 5).

Following Lewis and Reitz,[3] the thermoelectric power Θ_1 can be expressed in terms of plasma density and temperature. A convenient derivation is given in Ref. 13:

$$\Theta_1 = \frac{k}{e}\left\{\frac{4}{3} - \ln\left[\frac{n_e h^3}{2(2\pi m_e kT)^{3/2}}\right]\right\} \qquad (23)$$

The Seebeck emf of the thermocouple E_{12} is related to the thermoelectric power Θ_1 of the plasma

$$E_{12} = \int_{T_1}^{T_2}\Theta_1 dT \qquad (24)$$

Equation (23) indicates that Θ_1 is dependent on the temperature logarithmically; hence, one may assume an intermediate temperature. Then Eq. (21) can be written approximately as

$$E_{12} = \Theta_2(T_2 - T_1) \qquad E_{23} = \Theta_2(T_3 - T_2)$$

Note here that the thermoelectric power of the plasma is a thousandfold larger than that of the metal, because in the former the electrons are nondegenerate. Hence, in Eq. (23), the thermoelectric power is that of the plasma.

If one now neglects the effects of sheaths at the emitter or the collector, the open-circuit emf of the thermocouple will become

$$V_{0c} = \Theta_2(T_3 - T_1) \simeq \frac{kT_3}{e}\ln\left[\frac{n_e h^3}{2(2\pi m_e kT_3)^{3/2}}\right] - \frac{kT_1}{e}\ln\left[\frac{n_e h^3}{2(2\pi m_e kT_1)}\right] \qquad (25)$$

For the same assumptions, Eq. (9), derived independently from voltage-current considerations, will yield a similar result when one substitutes the saturation values for the electron currents, i.e.,

$$J_{th} = AT^2\exp\left(-\frac{e(\phi_E + V_{em})}{kT_1}\right)$$

$$J_{eem} = ne(kT/2\pi m_e)^{1/2} \quad \text{but } J_{th} = J_{eem}$$

Doing the same at the collector and assuming $T_{e1} \simeq T_1$, $T_{e2} \simeq T_3$,

$$V_{0c} = -kT_1\ln\left[\frac{n_e h^3}{2(2\pi mkT_1)^{3/2}}\right] + kT_3\ln\left[\frac{n_e h^3}{2(2\pi mkT_3)^{3/2}}\right]$$

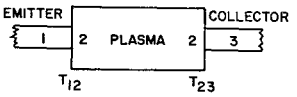

Fig. 5 Thermocouple sketch.

As noted previously, the plasma generator is a heat engine with a corresponding thermodynamic efficiency. This efficiency is given by the ratio of load power IV to the heat flux extracted from the cathode, or as the ratio of load power to the sum of load power and heat flux delivered to the anode,[12]

$$\eta = \frac{IV}{I_{th}[\phi_{em} + 2(k/e)T_{em}] - [I_{th} + I_{iem} - 1][\phi_c + 2(k/e)T_{e1}] + P_r} \qquad (26)$$

or, at the collector,

$$\eta = \frac{\text{IV}}{IV + I[\phi_c + 2(k/e)T_{e2}] + P_r} \qquad (27)$$

where P_r = radiation loss.

It should be noted that the collector (anode) heating, per electron, is given by $\phi_c + 2kT_{e2}$, and that this heating is the only inevitable collector heating. Furthermore, although the generator efficiency is less than a theoretical Carnot cycle efficiency, one should realize that useful power is being obtained from an otherwise wasted energy source, the shock-heated and ionized gas around a re-entry vehicle.

D. Power Output

To obtain an expression defining the power output of the generator, the emf of the generator is written after the manner of Sec. IA; thus,

$$E = \frac{kT_e}{e}\ln\left[\frac{1}{\beta}\left(\frac{I_{th} + I_{iem} - I}{I_{ic} + I}\right)\right] + \phi_E - \phi_c \qquad (28)$$

The power output then becomes

$$P = (E - Ir)I$$
$$P/I_{th} = (E - ir)i \qquad i = I/I_{th} \qquad (29)$$

To obtain the value of i for maximum power, one follows standard procedures for optimization which gives, for i_m, approximately

$$i_m = \frac{-[(b-a) + (V_T/E)(a+b) + (2abr/E)]}{2} + \left(\frac{[(b-a) + (V_T/E)(a+b) + (2abr/E)]^2 + 4ab}{2}\right)^{1/2} \qquad (30)$$

where $a = 1 + \gamma/\delta$ and $b = \gamma/\beta\delta$. Figure 6 is a plot of

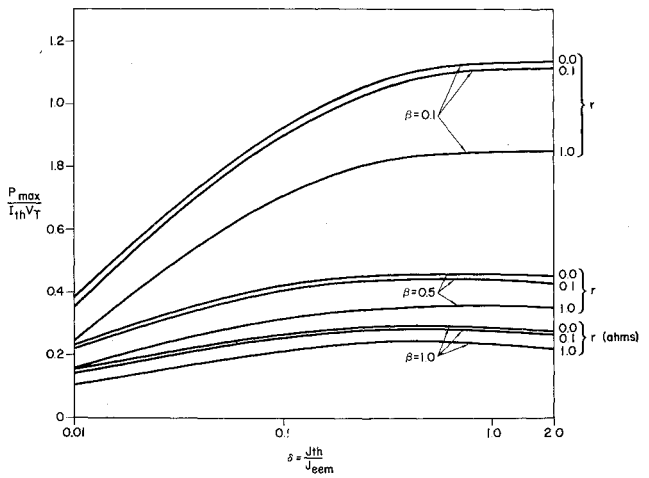

Fig. 6 Maximum power vs δ for various values of β and r.

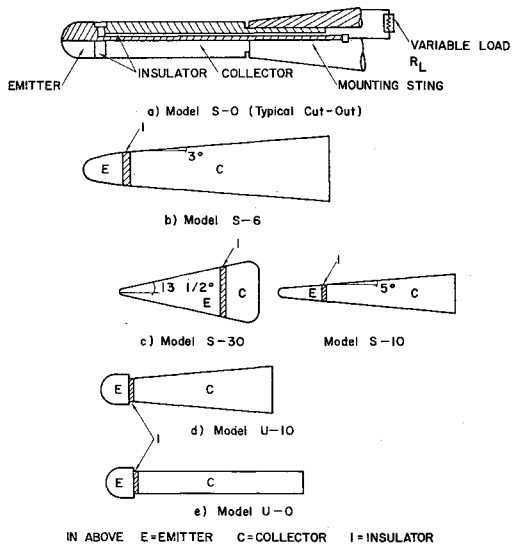

Fig. 7 Sketches of model generators for plasmajet.

maximum power, nondimensionalized by dividing it through product $I_{th} V_T$ vs the ratio of thermionic to random electron current δ for various internal impedances and emitter-to-collector area ratios. It is seen that the effect of internal resistance on maximum power output becomes more pronounced as β decreases and the maxima in all the curves shift to the right.

II. Experiment

To verify the analytical predictions of the hypersonic generator given previously, an extensive set of experiments were performed in the Sandia Corporation plasma arc tunnels with 160-kw and 1-Mw capacities. The various model geometries used in the plasma tunnels are shown in Fig. 7. The average diameter for the 160-kw jet was $\frac{3}{4}$ in. and, for the 1-mw jet, $1\frac{1}{2}$ in. A detailed description of the experiments and the results are given in Refs. 8 and 9. Some of the important aspects of these will be discussed below.

A. Factors Influencing Generator Output

From the generator theory discussed in Part I, one can deduce the following set of parameters that influence the generator power putput:

1. Emitter area

This parameter is directly proportional to the thermionic emission current, which in turn determines I_{sc} [see Eq. (12)] for a charge-neutralized plasma.

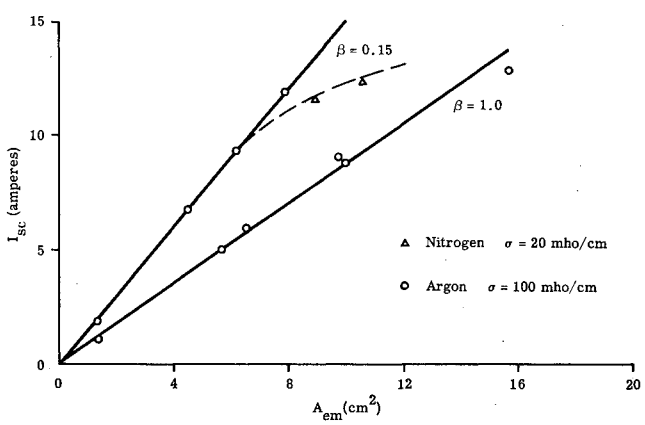

Fig. 8 Short-circuit current vs emitter area for two values of effective β.

2. Emitter-to-collector area ratio

This is the parameter β in Eq. (12).

3. Emitter and collector surface temperature

The Richardson Dushman equation shows that, the larger the emitter surface temperature, the greater is the electron emission rate. This, however, is controlled by the ion arrival rate given by Eq. (16). The effectiveness of a large emitter surface temperature is then dependent upon the plasma ionization level. A low collector temperature will reduce back emission possibilities.

4. Plasma ionization level and kinetic temperature

A high degree of ionization affects the generator output by neutralizing the electron space charge at the emitting surface and improving plasma conductivity. The open-circuit voltage depends on ionization levels through the term γ in Eq. (11). The effect of high-plasma kinetic temperature is to increase voltage output proportionately.

5. Plasma resistance and contact resistance

These two constitute the internal impedance of the circuit and, because the hypersonic generator is a relatively high-current/low-voltage device, both should be kept at a minimum.

6. Emitter and collector material

These enter through the work function terms appearing in the Richardson-Dushman equations. In a pure thermionic emitter these are of great importance. In a reactive atmosphere not much can be done to control the work functions; nevertheless, a low ϕ_{em} and a large $\phi_{em} - \phi_c$ would be beneficial for the generator output as seen from Eq. (5).

Obviously, there is a strong interdependence among the various parameters just listed. A favorable effect expected by a change in one parameter might cause an adverse effect on a second parameter and thus reduce the net output. The following results, compared with theoretical predictions, attempt to establish optimum working conditions for the hypersonic plasma generator.

B. Experimental Results

The average flow Mach number in the Sandia Corporation 160-kw jet was 2.5 with maximum jet enthalpies of 6000 Btu/lb for argon and 14,000 Btu/lb for air (or nitrogen). The ambient pressure in the test chamber was of the order of 7 mm (~0.01 atm), and stagnation pressures ranged from 0.06 to 0.13 atm.

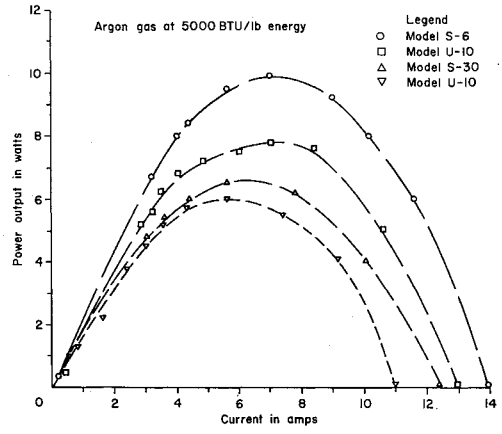

Fig. 9 Power output for various model geometries at constant jet energy.

1. *Emitter area*

Model emitter areas varied between 5 and 20 cm². Figure 8 shows plots of short-circuit current vs emitter area. As predicted from Eq. (12), the results show a linear dependence of I_{sc} on emitter area. According to Eq. (31) this linear dependence should change as the plasma resistance becomes significant ($r_p > 0.01$ ohm). This effect was noticed clearly in nitrogen, but was insignificant in argon for the model sizes tested, because of the high degree of ionization in the latter. Also as expected, the open-circuit voltage V_{0c} was independent of emitter or collector area.

2. *Emitter-to-collector area ratio*

A large number of runs were made to determine the effect of β on power output, especially on the short-circuit current I_{sc}. Figure 8 shows this effect graphically. As expected, for $\beta < 0.1$, little or no difference could be noticed in I_{sc}. The influence of β could be isolated from contact resistance anomalies and flow separation effects only for relatively few cases. Consequently, an "effective" β was defined by taking into account the actual "wetted" area of the collector, as observed visually and the internal contact resistance. Values of β isolated from the preceding errors could be obtained only for joints contacting through a liquid medium (see below) and for conical afterbodies.

3. *Emitter and collector surface temperature*

Surface temperatures were measured by means of a two-color pyrometer attached to a recording chart. Whenever the arc glow overshadowed surface color temperature, the jet was turned off and the surface temperature estimated from the time-temperature decay history, with an accuracy not better than ±100°C. Depending on the arc, jet energy T_{em} varied between 2300° and 3400°C, and T_c varied between 1200° and 2000°C. For optimum output, the collector to emitter surface temperature ratio had to be less than 0.8 to reduce back emission. This was experimentally determined by varying the collector cone angle from 0° to 30°. Figure 9 shows the output for four such geometries having approximately the same A_{em} and β. There is a noticeable decrease in power output for cone angles above 20° and for hammerhead geometries with reduced "wetted" area because of flow separation.

4. *Plasma ionization level and kinetic temperature*

These by far are the two most important factors affecting generator output. Spectroscopic measurements indicated approximately 1-ev electron temperatures at a jet energy input of 5000 Btu/lb. The ionization rate could be varied more or less independently of electron temperature through small amounts of seeding or by using various gas mixtures. Figure 10 shows the sharp drop in short-circuit current output with decrease in argon content in the arcjet. The degree of ionization in argon was estimated from spectroscopic measurements[13] to be 2–5 × 10^{16} electrons/cm³, and for the same energy input in nitrogen, 2 × 10^{13}/cm³. These results underscore the necessity for complete space charge neutralization as a requisite for useful generator output. Power seeding with K

Table 1 Calculated open-circuit voltage

	Argon		Air	
	δ	V_{0c}	δ	V_{0c}
$V_{em} < 0$	0.10	0.10	0.10	1.92
	0.01	1.37	0.01	0.67
$V_{em} > 0$	0.10	6.51	0.10	4.22
	0.01	5.95	0.01	2.03

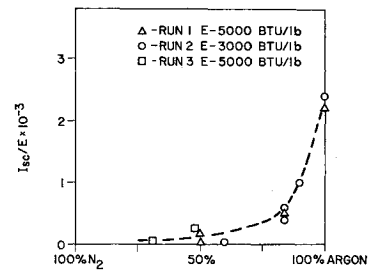

Fig. 10 Degree of ionization on short-circuit current output: argon-nitrogen mixtures.

or Cs had much the same effect on the short-circuit current, being more pronounced in nitrogen or air than in argon. Figure 11 shows I_{sc} as a function of estimated electron density. The open-circuit voltage depends on the ionization level through the terms δ and γ as seen from Eq. (11). Maximum value of γ^{-1} for argon is 293 and for air 155 under complete space charge neutralized conditions. On the other hand, δ can vary anywhere from less than 10^{-2} to about 2, depending on the thermionic emission rate and plasma ion density. Under optimum arcjet conditions and minimum contact resistance, the maximum value in measured V_{0c} was about 3.5 v in argon. From Eqs. (10) and (11), Table 1 is obtained for argon ($V_T = 1$ ev, $\gamma = \frac{1}{293}$) and for air ($V_T = 0.7$ ev, $\gamma = \frac{1}{155}$). The values for δ throughout the experiments were within the preceding limits and the V_{0c} magnitudes corresponded to those given by Eq. (9), $V_{em} < 0$.

Three types of seed materials were used, KCl, K_2CO_3, and cesium. Because of the electronegative properties of KCl, where V_{0c}-seeded gave 10% lower values than V_{sc}-no-seed, the KCl was discarded. K_2CO_3 powder was fed downstream of the arc at the rate of 1 g/min, or a maximum of 1% by weight of the gas mass flow rate. An increase of 15–25% in the value of V_{0c} was obtained because of seeding, whereas I_{sc} increased as much as 100% (see Fig. 11). A recent set of experiments were completed with cesium-impregnated tungsten emitters. Much more efficient seeding was obtained in this manner with a factor of 2 or more increase in output over the K_2CO_3 seeding process.

5. *Plasma and contact resistance*

On the basis of ionization level and electron temperature estimates, plasma conductivities in argon were above 50 mho/cm and in air about 5 mho/cm. The latter was calculated by the method of Ref. 14 (see Ref. 8). When insulator lengths were varied from 0.2 to 3.0 in., no change in output could be noticed in argon; but I_{sc} fell by 15% in air or nitrogen, indicating the limiting value of plasma resistance on current output. This can be seen from the expression for the short-circuit current when the plasma resistance term r is included, i.e.,

$$Ci_{sc} = \ln[(1 + \gamma/\delta + i_{sc})/(\gamma/\delta + \beta i_{sc})] \qquad (31)$$

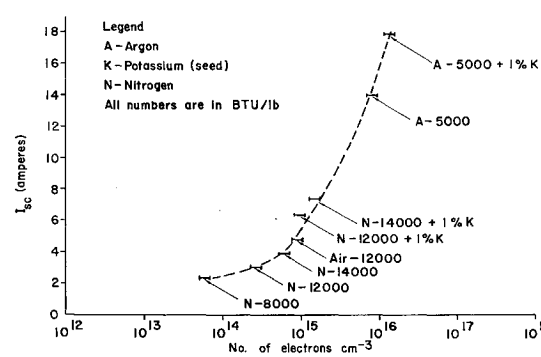

Fig. 11 Short-circuit current vs electron density (values from spectroscopy).

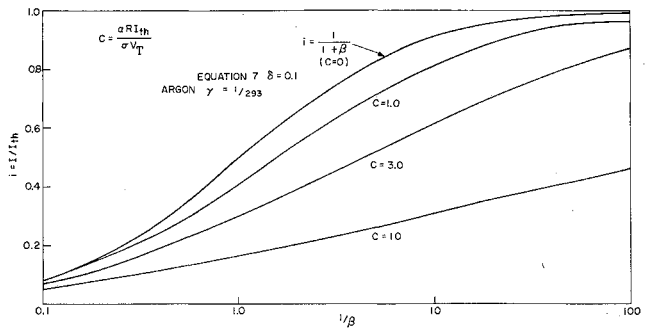

Fig. 12 Dimensionless short-curcuit current vs $1/\beta$ for various resistance parameters C in argon and in air.

where $C = \alpha R I_{th}/\sigma V_T$. Equations (12) and (31) are plotted in Fig. 12. It is clearly seen that, for a given β, the short-circuit current falls below the $r_p = 0$ value if plasma resistance is included. Largest impedances however came from the various contact points in the typical model (see Fig. 7a). These were finally minimized by using liquid contact (cadmium solder and Tl-Hg-In liquid metal alloy) between collector and sting mount and emitter and connecting tungsten bolt. Under these conditions, r varied between 0.08 and 0.12 ohm.

6. *Emitter and collector material*

All possible refractory materials were tested either as emitters or collectors. Characteristics predicted for optimum output were general thermal resistance and mechanical integrity, good electrical conductivity, and a low thermionic work function. Of these three, experiments showed the last to be the least important since not much could be done to preserve surface integrity in a highly reactive atmosphere such as dissociated-ionized air. Some of the materials tested, with ionized air as the working gas in the arcjet, were tungsten, thoriated tungsten, molybdenum, niobium, graphite, pyrolitic graphite, phenolic impregnated with carbon, and hafnium (zirconium) carbide. All but the last four of these lost their high-power output characteristics when various oxide layers covered the collector surfaces (1000°–1500°C) and served as insulators after 15 sec of run time. Graphite or pyrolitic graphite emitter-collector combinations showed steady output and good mechanical integrity. Insulator materials were selected chiefly for their thermal shock properties. Boron nitride and 99% alumina dispersed with 5% by volume molybdenum turned out to be quite adequate.

C. Optimum Results

Data reduction showed that blunted cone emitters (0.25-in.-diam radius) which were followed by 6°–10° conical afterbodies, $\beta \leq 0.15$, and ATJ graphite or tungsten surfaces yielded the highest output (Fig. 13). The maximum short-circuit current measured was 24 amp over a hemispheric emitter of $\frac{3}{8}$-in. radius at 3250°K. According to the Richardson-Dushman equation, this value should be 78 amp for the constant $A = 120$. However, if one assumes T_{em} to be a function of θ, the azimuthal angle, and assumes a parabolic temperature drop from stagnation point, $\theta = 0$ to $\theta = \pi/2$ (Fig. 4), Eq. (14) will yield a value for $I_{th} = 27$ amp. This is much closer to the measured value of 28 amp. Table 2 summarizes the optimum outputs per emitter area for several different materials, both in argon and in air.

Two things are obvious from Table 2. First, phenolic carbon is seen to average about 70% of the short-circuit current of graphite and 60% of the power output with no significant change in open circuit voltage. The former two show the effect of internal impedance offered by the material, and the latter points to the fact that V_{0c} depends primarily on the plasma energy. Second, comparing the S-6 shape with $\beta = 0.1$ with the S-30° sharp-cone model with $\beta = 1$, it is easy to see how a large collector-to-emitter area ratio (small β) affects output in the case of argon. However, this ratio is more than compensated for in air because of its low plasma conductivity.

The highest short-circuit current recorded in argon was 28 amp/in.^{2} of emitter area, and the highest open-circuit voltage recorded was 4.4 v. In air (80% N, 20% 0), the corresponding values were 8 amp/in.^{2} and 2.3 v, respectively. After seeding with cesium (impregnated in tungsten emitters), these values increased to 20 amp/in.^{2} and 4.2 v (20 w/in.^{2}). Repeatability of runs for identical models were governed chiefly by reliability of consecutive runs in the plasma jet and repeatability of contact resistance. Under best conditions of control, repeatability varied between 10–25%. When contact resistance was under close control, low arcjet reliability was caused primarily by electrode erosion.

D. Free-Flight Conditions

It is difficult to assess the exact range of applicability of plasmajet experiments to free-flight conditions where the air is shock ionized and has comparatively lower kinetic temperatures than those found in an arcjet. A set of prototype

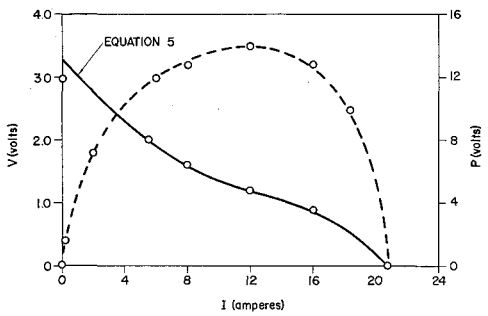

Fig. 13 Output data for $\beta = 0.15$, $V_T \sim 0.8$ $\delta = 0.01$, in argon gas at 6000 Btu/lb.

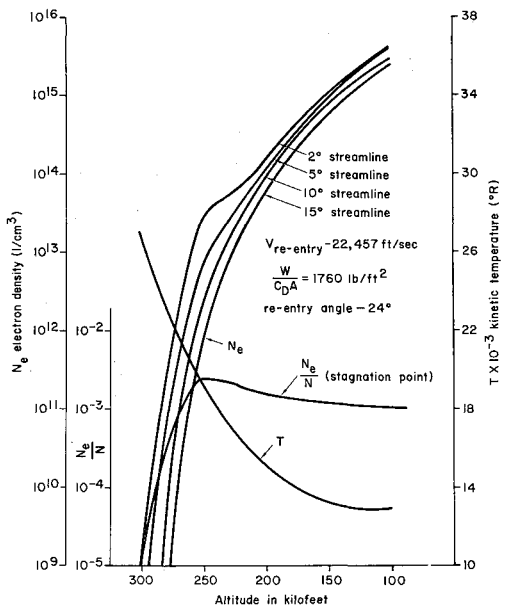

Fig. 14 Electron density and kinetic temperature near stagnation point for blunt re-entry vehicle at various altitudes.

Table 2 Optimum output per emitter area (without plasma seeding)

Model	Material	5000 Btu/lb			12,000 Btu/lb		
		I_{sc}, amp/in.^{2}	V_{oc} v	Maximum power, w/in.^{2}	I_{sc}, amp/in.^{2}	V_{oc}, v	Maximum power, w/in.^{2}
S-6 (12° blunted cone) $\beta = 0.15$	Graphite (emitter, collector)	21	3.25	15	4.0	1.3	2.3
	Phenolic carbon emitter, graphite collector	15	3.25	8	3.0	1.0	1.5
S-30° (sharp cone) $\beta = 1$	Tungsten (emitter collector)	13	3.20	7	4.5	1.7	2.3
	Phenolic carbon (emitter collector)	...	...	...	3.8	1.4	1.4

re-entry vehicles from graphite and pyrographite are being prepared to be carried along and ejected from Atlas missiles to check the final feasibility of this generator concept. Extensive aerodynamic calculations on an Atlas trajectory have been made by TRW Space Technology Laboratories for Sandia Corporation, and estimates of ionization levels, prototype surface temperatures, and electron temperature have been obtained. Figure 14 is one plot for optimum electron concentration and kinetic temperature for a blunt body re-entering at 22,000 fps. Under no-seed conditions with $\beta = 0.1$, this vehicle is estimated to yield some 25 w of power through a matched load of 0.1 ohm between altitudes of 250 to 100 kft. The short-circuit current, translated from the plasmajet air runs, could yield as much as 100 amps for a 5-in.-diam vehicle. This means that one would need a larger potential to drive these thermionic currents by either dividing the vehicle surface into several emitter-collector pairs or by using supersatellite re-entry speeds generating 6–10 v of open-circuit voltage. Either of these will cause the output of a full-size re-entry vehicle (3.0 ft in diameter) to be 1 kw or more.

Stagnation pressures above 1 atm establish the lower limit (in altitude) for the operation of the hypersonic generator because of a sharp reduction in thermionic current. For an average re-entry vehicle, this corresponds to an altitude of 120,000 ft and less.

Conclusions

Admittedly, the analyses presented previously are at best approximate. However, most of the parameters discussed seem to be in good agreement with experiments. A new set of experiments with better measurement techniques will hopefully permit us to present better quantitative results for plasma resistance effects on power output.

Because of its simplicity and the use of otherwise wasted energy, the hypersonic plasma power generator, with very minor design modification, may have useful applications as an auxiliary power supply, especially in supersatellite re-entry trajectories and in planetary atmospheres.

References

[1] Nottingham, W. B., "Thermionic emission," Ann. Physik **21**, 1–175 (1956).

[2] Carabateas, E. N., Pezaris, S. D., and Hatsopoulos, G. N., "Interpretation of experimental characteristics of cesium thermionic convertors," J. Appl. Phys. **32**, 352–358 (1961).

[3] Lewis, H. W. and Reitz, J. R., "Thermoelectric properties of the plasma diode," J. Appl. Phys. **30**, 1439–1445 (1959).

[4] Fatmi, H. A., "A new thermionic generator with ion injection," *Proceedings of the 4th International Conference on Ionization Phenomenon in Gases* (North-Holland Publishing Co. Amsterdam. Holland, 1961).

[5] Waymouth, J. F., "Electrical energy from high-temperature plasmas," Inst. Elec. Electron. Engrs. J. **8**, 380–383 (1962).

[6] LeBlanc, A. R., "Hypersonic plasma thermionic generator," Parts I and II, Sandia Corp. Rept. SC-DC-2848 (August 1962); also Univ. of New Mexico Engineering Experimental Station, TR EE-81 (August 1962.)

[7] Cotter, T., "Hypersonic plasma thermocouple," Los Alamos Scientific Lab. LASL LAMS-2481 (January 1961).

[8] Touryan, K. J., "The hypersonic plasma converter: I," Sandia Corp. Research Rept. SC-4960(RR) (January 1964).

[9] Touryan, K. J., "The hypersonic plasma converter: II," Sandia Corp. Research Rept. SC-RR-64-979 (November 1964).

[10] Langmuir, I., "The interaction of electron and positive ion space charges in cathode sheaths," Phys. Rev. **33**, 954–989 (1929).

[11] S. H. Lam, "A general theory for the flow of weakly ionized gases," AIAA J. **2**, 256–262 (1964).

[12] Lewis, H. W. and Reitz, J. R., "Efficiency of the plasma thermocouple," J. Appl. Phys. **31** (1960).

[13] Shipley, K. L., "Spectrographic analysis of plasma jets," Sandia Corp. Research Rept. SC-4776(RR) (March 1963).

[14] Shkarofsky, I. L., Bachynski, M. P., and Johnston, T. W., "Collision frequency associated with high temperature air and scattering cross-sections of the constituents," Planet. Space Sci. **6**, 24–46 (1961).